

---

# Homo- and heteronuclear alkali metal trimers formed on helium nanodroplets. II. Femtosecond spectroscopy and spectra assignments

Christian Giese<sup>a</sup>, Frank Stienkemeier<sup>a</sup>, Marcel Mudrich<sup>a</sup>, Andreas W. Hauser<sup>b</sup> and Wolfgang E. Ernst<sup>c</sup>

Homo- and heteronuclear alkali quartet trimers of the type  $K_{3-n}Rb_n$  ( $n = 0, 1, 2, 3$ ) formed on helium nanodroplets are probed by one-color femtosecond photoionization spectroscopy. The obtained frequencies are assigned to vibrations in different electronic states by comparison to high level *ab initio* calculations of the involved potentials including pronounced Jahn-Teller and spin-orbit couplings. Despite the fact that the resulting complex vibronic structure of the heavy alkali molecules complicates the comparison of experiment and theory we find good agreement for many of the observed lines for all species.

## 1 Introduction

Helium nanodroplet isolation (HENDI) spectroscopy has become an established technique for producing and probing molecules, clusters, and chemical reactions at low temperatures.<sup>1-4</sup> Dopant species are cooled down to the internal temperature of the droplet (0.37 K)<sup>5</sup> and readily form complexes, weakly bound ones being favored.<sup>6</sup> Due to their low binding energy, high-spin alkali-metal molecules are hardly accessible in conventional gas-phase experiments but are preferentially formed on helium droplets.<sup>6-8</sup> Alkali atoms, molecules and clusters in high-spin states have been extensively studied by cw<sup>9-14</sup> and time-resolved spectroscopy.<sup>2,15-22</sup>

Although helium is the least perturbing solvent and helium nanodroplets are often referred to as a nearly ideal spectroscopic matrix, electronic spectra of atoms or molecules in or on He droplets are still strongly broadened. On the one hand, this is a severe limitation as to the precision of ro-vibrational spectra as compared to gas-phase spectroscopy. On the other hand, valuable information about the interaction of the dopant with the droplet may be obtained from helium perturbations.<sup>23-28</sup> Significantly improved spectral resolution can be achieved by time-domain spectroscopy using the femtosecond pump-probe technique<sup>20,22</sup> or by measuring fine and hyperfine structure directly in the microwave regime<sup>29</sup>.

In previous experiments, high-spin alkali trimers formed on helium nanodroplets have been interrogated using laser spectroscopy<sup>8,30,31</sup> as well as sophisticated variations thereof in order to separate spectrally overlapping bands of various trimer

species.<sup>12,32-34</sup> In the case of  $Na_3$  and  $K_3$ , excitation and emission spectroscopy allowed for vibrational resolution.<sup>8,30,31,34</sup> High-spin alkali trimers are particularly interesting model systems for studying nonadiabatic transitions from weakly bound van der Waals aggregates to covalently bound metallic clusters.<sup>35-37</sup> Upon electronic excitation of high-spin  $Na_3$  and  $K_3$  formed on helium droplets into the  $2^4E'$ -state, the quartet trimers undergo intersystem crossing to the doublet manifold followed by dissociation into singlet dimers and single atoms.<sup>7,31</sup>

Alkali trimers in their doublet states were investigated at very high resolution, which allowed to derive details of Jahn-Teller and pseudo Jahn-Teller interactions from the splitting of rotational states.<sup>38,39</sup> As trimers in their weakly bound quartet states have only been observed on helium droplets, such high resolution has not been achieved in the optical spectroscopy range. As a complementary approach to spectroscopy with vibronic resolution the femtosecond pump-probe technique can be applied, as was demonstrated for the doublet trimers  $Na_3$  and  $K_3$ .<sup>40-45</sup> This technique relies on the creation and probing of a coherent superposition of vibrational states (wave packet, WP) in the time domain. Subsequent Fourier analysis yields information about difference frequencies between the coherently excited states. The advantage with respect to cw spectroscopy is that spectral information can be gained even in strongly perturbed systems that are subject to fast dissociation or to interactions with an environment. Thus, by using femtosecond pump-probe spectroscopy, it was possible to measure vibrational frequencies of the previously unobserved dissociative B-state of the  $K_3$  trimer,<sup>41,45</sup> which was later confirmed in *ab initio* calculations.<sup>46</sup> At high laser intensity, additional vibrational WP dynamics in the ground state was observed induced by resonant impulsive Raman scattering (RISRS).<sup>40,44,45</sup> The femtosecond dynamics of  $Na_3$  in the B-state was found to be dominated by the symmetric stretch mode  $Q_s$  in contrast to cw measurements.<sup>42,44,45</sup> This mode

---

<sup>a</sup> Physikalisches Institut, Universität Freiburg, 79104 Freiburg, Germany. E-mail: marcel.mudrich@physik.uni-freiburg.de, christian.giese@physik.uni-freiburg.de

<sup>b</sup> Centre for Theoretical Chemistry and Physics, The New Zealand Institute for Advanced Study, Massey University, 0745 Auckland, New Zealand. E-mail: andreas.w.hauser@gmail.com

<sup>c</sup> Institute of Experimental Physics, Graz University of Technology, Petersgasse 16, A-8010 Graz, Austria. E-mail: wolfgang.ernst@tugraz.at

decays within a few picoseconds due to intramolecular vibrational redistribution (IVR) to the two other modes. Note, however, that the excitation of vibrational modes was found to be quite selective depending on the laser pulse parameters, in particular the pulse duration.<sup>40,41,43,44</sup> On the one hand, this offers the opportunity of accessing vibrational modes that are not excited by cw laser excitation, in particular when using short and intense pulses.<sup>40,44</sup> On the other hand, this can hamper the direct comparison of the Fourier spectra obtained from femtosecond or picosecond pump-probe transients with cw excitation spectra. Besides, additional fine structure effects induced by *e.g.* spin-orbit coupling, rotations, or matrix interactions, which naturally appear as line splittings, shifts and broadenings in absorption or emission spectra, are not directly probed by pump-probe vibrational coherence spectroscopy.<sup>22,47</sup> Femtosecond pump-probe spectroscopy has been applied to alkali atoms and molecules attached to helium nanodroplets by our group in a series of experiments.<sup>2,20–22</sup> Besides obtaining a wealth of dynamical information, high-resolution spectra of diatomics have been extracted that give insight into the subtle couplings of the vibrating molecules to the helium droplet surface.<sup>27,28</sup>

Due to the small size and the simple valence structure of the constituents, alkali trimers are particularly attractive as benchmark systems for accurate theoretical treatment. Besides the mentioned spin-orbit couplings the Jahn-Teller (JT) effect, specifically the problem of  $E \otimes e$  vibronic coupling, has been a matter of high interest and continuous research.<sup>34,48</sup> The calculation of accurate potential energy surfaces (PES) for trimers formed of the heavy alkali elements is computationally quite demanding. However, with the advances in computational power and techniques, PES for homo- and heteronuclear alkali trimers involving potassium, rubidium and cesium have recently been determined by several groups.<sup>12,34,36,48,49</sup> Besides, alkali trimers in quartet states are particularly well suited for studying nonadditive three-body interaction terms, which represent significant contributions to the binding energy.<sup>30,50</sup>

Recent advances in forming ultracold molecules by photo- or magneto-association through Feshbach resonances using trapped samples of ultracold atoms has stimulated increasing demand for accurate PES of three-atomic systems. In particular, schemes for stabilizing initially highly excited molecules into low-lying levels are based on the precise knowledge of molecular structure and spectra.<sup>51–53</sup> Moreover, accurate triatomic PES are required in the emerging field on ultracold chemistry.<sup>54–58</sup>

In this work we present one-color femtosecond pump-probe spectroscopy of homo- and heteronuclear quartet alkali trimers of rubidium and potassium atoms. Vibrational frequencies of excited and ground state trimers in all possible combinations of species are extracted and compared to high-

level quantum chemical calculations. In addition, the real-time dynamics of individual frequency components is analyzed. The article is organized as follows: After a short description of the apparatus the experimental results are presented and data analysis is exemplified for  $\text{Rb}_3$ . This is followed by a theoretical part summarizing the findings of our previous *ab initio* calculations on these systems<sup>34,35,48</sup> and makes extensive use of the data provided in the closely connected Ref. 59, which is referred to as Paper I throughout this article. The final section is dedicated to the discussion and interpretation for all studied trimers  $\text{Rb}_3$ ,  $\text{KRb}_2$ ,  $\text{K}_2\text{Rb}$  and  $\text{K}_3$  are presented based on the theoretical spectra simulations.

## 2 Experimental

The details of the experimental setup have been described in previous publications.<sup>9,22</sup> Helium droplets are formed in the expansion of helium at high pressure ( $\sim 50$  bar) out of a cold nozzle ( $T = 15$  K, diameter  $d = 5 \mu\text{m}$ ). In two stainless steel pickup cells, a number Rb and K atoms are attached to the droplets according to the pickup statistics at a given vapor pressure.<sup>60</sup> Doping-cell temperatures are adjusted to achieve highest formation rates of trimer species and are listed in Table 1.

Alkali atoms and molecules are peculiar dopants in that they reside in weakly bound dimple-like states at the surface of helium nanodroplets.<sup>7,61–63</sup> Because of the high mobility on the helium surface homonuclear clusters ( $\text{Rb}_3$  and  $\text{K}_3$ ) and heteronuclear clusters ( $\text{KRb}_2$  and  $\text{K}_2\text{Rb}$ ) are formed when doping one droplet with three atoms. Upon cluster formation, the binding energy is dissipated by evaporation of helium atoms which leads to the depletion of strongly bound clusters and to an enrichment of the weakly bound high-spin clusters, *i.e.* alkali trimers in the lowest quartet state. According to recent simulations of the formation of alkali clusters on helium droplets<sup>60</sup>, we expect a contribution of doublet trimers on the order of  $\sim 10\%$  with respect to the high spin molecules. However, so far no low spin trimer states have been identified in cw spectra of alkali trimers attached to helium droplets. Therefore, all observed frequencies discussed in section 4 are related to quartet states. In the presented femtosecond pump-probe measurements, we can not definitely rule out doublet trimers to contribute to the spectra.

As an example, the doublet ground state have potential of  $\text{Rb}_3$  ( $1^2E'$ ) has a formation energy of about  $5321 \text{ cm}^{-1}$  as compared to  $939 \text{ cm}^{-1}$  for the  $1^4A'_2$  lowest quartet state.<sup>34,48</sup> Thus-formed trimers immediately thermalize to the nanodroplet equilibrium temperature (370 mK) such that only the vibrational ground state ( $v = 0$ ) and a few rotational states are populated. Thus, helium nanodroplet isolation (HENDI) is an ideal method for species and state preparation to perform single quantum channel experiments.

**Table 1** Pick up cell temperatures for optimum trimer formation.

Species	$T_{Rb-oven}$ [° C]	$T_{K-oven}$ [° C]
Rb <sub>3</sub>	115	-
Rb <sub>2</sub> K	103	115
RbK <sub>2</sub>	83	130
K <sub>3</sub>	-	140

The laser system consists of a Ti:Sapphire femtosecond oscillator (Chameleon series/Coherent) that produces Fourier limited pulse trains over a broad spectral range of 700–1050 nm (9500–14300 cm<sup>-1</sup>) at 80 MHz pulse repetition rate with a cw output power of 1-3 W. For the chosen excitation frequencies, the laser pulse lengths are about 160 fs, yielding a spectral full width at half maximum (FWHM) of about 80 cm<sup>-1</sup>. Pulse pairs are created with a Mach-Zehnder type interferometer where a commercial delay stage (Newport) is placed in one of the arms. In this way the time delay between the pulses is controlled with sub-femtosecond precision. The droplet beam is crossed with the laser beam at ninety-degree angle inside the active volume of a commercial quadrupole mass spectrometer (Extrel) and the formed molecular ions are recorded in counting mode as a function of the delay time.

## 2.1 Vibrational femtosecond pump-probe spectroscopy of triatomic molecules

Vibrational WP dynamics is probed by applying pairs of identical laser pulses with variable delay. The first ‘pump’ pulse excites a coherent superposition of vibrational states in a well defined region of the molecular PES according to the laser bandwidth and the overlap of ground and excited state wave functions (Franck-Condon (FC)-factors). The created WP starts to propagate on the PES until the second ‘probe’ pulse projects it onto a detection state (ionic or fluorescent) after a delay time  $\Delta t$ . According to the Franck-Condon principle, transitions between electronic states are energetically allowed at molecular coordinates at which the laser energy matches the energy gap between ground and excited state PES (‘Condon points’) and transition probabilities are determined by the FC-factors. Well-localized FC-regions in coordinate space (‘FC-windows’) are essential for filtering out the WP dynamics and for obtaining oscillatory ion yields as a function of  $\Delta t$  with high contrast.<sup>20</sup> Such regions are mostly located at classical turning points of the molecular vibration.

Based on previous measurements of vibrational WP dynamics in potassium and rubidium dimers, we expect essentially two possible excitation pathways to contribute to the pump-probe signal.<sup>20,22</sup> In the first case, the pump pulse populates states in an excited quartet potential, and the probe pulse ionizes the molecule by a two-photon transition. In the second case, the high intensities of the ultrashort laser pulses in-

duce resonant impulsive stimulated Raman scattering (RISRS) which creates WPs in the initial quartet ground state. Since the vibrational WP oscillates in the symmetry adapted coordinates of the molecules, the recorded ion yield is also periodically modulated, depending on the number of Condon points and on FC-factors. In a harmonic potential the oscillation is undamped and will therefore only be limited by the lifetime of the involved vibronic states, whereas in anharmonic PES the WP undergoes dispersion. This leads to the spreading of the WP and to the loss of contrast of the pump-probe signal. This process is reversible, though, and after characteristic delay times the WP rephases to form so-called revivals, as nicely seen in pump-probe spectra of Rb<sub>2</sub>.<sup>22</sup> Irreversible dephasing can be induced either by population decay from the initially prepared vibronic states by spontaneous emission, inter-system crossing, internal conversion, or by dissipative interactions with the environment (the helium droplets in our case). In addition, system-bath coupling may cause pure dephasing by elastic interactions without dissipation.<sup>27</sup>

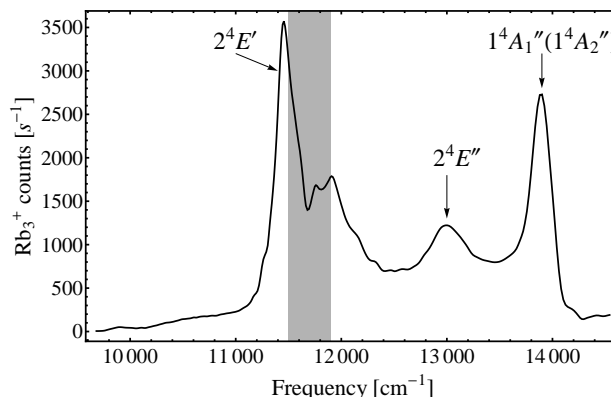


**Fig. 1** Photoionization spectrum of rubidium trimers Rb<sub>3</sub> recorded by tuning the femtosecond laser. WP oscillations were observed within the shaded area.

In a first step, photoionization (PI) spectra using single laser pulses are recorded for all observed trimer species in order to explore the excitation bands and to find suitable wavelength regions for pump-probe measurements. The PI spectrum of rubidium trimers Rb<sub>3</sub> is shown in Fig. 1 for illustration. Three main features around 11500 cm<sup>-1</sup>, 13000 cm<sup>-1</sup>, and 14000 cm<sup>-1</sup> can be assigned to resonant transitions  $2^4E' \leftarrow 1^4A_2'$ ,  $2^4E' \leftarrow 1^4A_2''$ , and to  $1^4A_{1,2}'' \leftarrow 1^4A_2'$ , respectively.<sup>35</sup> The transition  $2^4E' \leftarrow 1^4A_2'$  has been extensively studied by laser-induced fluorescence (LIF) and magnetically-induced circular dichroism (MCD) spectroscopy.<sup>32-34</sup> Pump-probe transients have been recorded at all laser wavelengths at which the photoionization yield is maximum but clear WP oscillations are observed only in the frequency interval 11500–

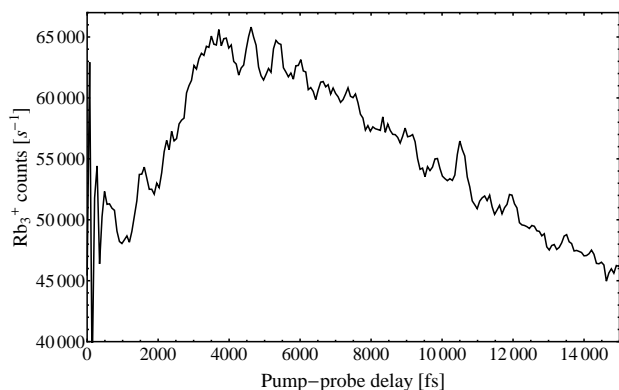


**Fig. 2** Typical pump-probe photoionization transient recorded at the mass of  $\text{Rb}_3$  at a laser wavelength of 850 nm ( $11765 \text{ cm}^{-1}$ ). The oscillatory pump-probe signal is superimposed by a slowly varying offset resulting from photo-fragmentation.

$11900 \text{ cm}^{-1}$  (indicated as shaded area in Fig. 1). The corresponding pump-probe transients are discussed in detail in Sec. 4.

Let us exemplify the analysis of the pump-probe data with the help of the  $\text{Rb}_3$ -transient recorded at  $\lambda = 850 \text{ nm}$  ( $11765 \text{ cm}^{-1}$ ) depicted in Fig. 2. It is composed of two parts: The oscillatory pump-probe signal contains the information about the vibrational WP dynamics. In addition, the ion yield slowly increases within the first few picoseconds before decreasing on a longer timescale. The initial increase of the ion signal level results from photo-fragmentation of larger clusters into the trimer channel which does not contribute to the coherent WP dynamics.<sup>45,64,65</sup> The subsequent dissociation of the trimers into dimers and atoms leads to the drop of signal level at later delay times. Similar photo-fragmentation dynamics of small alkali clusters in low-spin states in the gas-phase have been studied in detail.<sup>41,45</sup> By fitting an exponential decay model to the falling edge of the transient data, a dissociation time constant of  $\tau_d = 8.9(08) \text{ ps}$  can be inferred, somewhat longer than the dissociation times  $\tau_d = 4\text{--}7 \text{ ps}$  found for low-spin  $\text{K}_3$  in the B-state.<sup>41</sup>

In order to extract the involved vibrational frequencies, the data are Fourier transformed after removing the slowly varying envelope using a high-pass filter ( $15 \text{ cm}^{-1}$  cutoff frequency). This filtering also removes other longterm signal variations not related to WP-dynamics, mainly drifts of room and nozzle temperature. We therefore do not attempt to assign expected low-frequency components. The resulting power spectrum of  $\text{Rb}_3$  recorded at 850 nm ( $11765 \text{ cm}^{-1}$ ), depicted in Fig. 3, contains a few clearly discernable lines. Line positions, widths and amplitudes are analyzed in Sec. 4 and are assigned to vibrational modes by comparing with model calculations (Sec. 3). Unassigned lines are marked with stars,

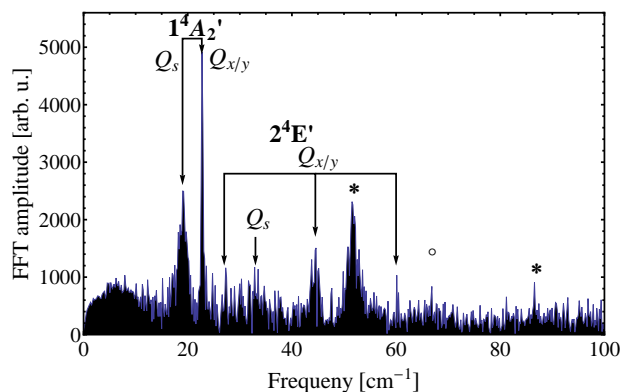


**Fig. 3** Power spectrum of the  $\text{Rb}_3$  pump-probe photoionization transient recorded at the laser wavelength 845 nm ( $11834 \text{ cm}^{-1}$ ). Unassigned lines are marked with a star and overtone frequencies with a circle.

and overtone frequency of assigned lines with circles.

As a unique feature of pump-probe spectroscopy, information about the temporal behavior of the spectral components is accessible. By Fourier transforming the data using the sliding window technique, so-called spectrograms can be generated, which contain both spectral as well as temporal information.<sup>44</sup> Fig. 4 displays the spectrogram obtained from Fourier analyzing the pump-probe data of  $\text{Rb}_3$  (Fig. 2) using a Gaussian window function with a full width at half maximum of 15 ps. For better visibility the data is plotted with a square root contour function. The frequency components at about  $23 \text{ cm}^{-1}$  and  $45 \text{ cm}^{-1}$ , which are assigned to the asymmetric stretch and bending modes  $Q_{x/y}$  of electronic states  $1^4A'_2$  and  $2^4E'$ , respectively, are clearly visible up to delay times  $\Delta t \gtrsim 200 \text{ ps}$ , whereas the symmetric stretch mode  $Q_s$  in the same states at frequencies  $19 \text{ cm}^{-1}$  and  $33 \text{ cm}^{-1}$ , respectively, disappear within less than 20 ps. The pronounced difference in dephasing times between symmetric and asymmetric vibrational modes, which is consistently observed with all other trimer combinations, may be due to intramolecular vibrational redistribution (IVR) as observed with low-spin  $\text{Na}_3$  excited to the B-state.<sup>44,45</sup> In order to ascertain this hypothesis quantum dynamics calculations would have to be performed.<sup>42,43</sup>

Beside this effect, in high-spin trimers attached to helium nanodroplets, additional dynamics may occur due to quartet-doublet intersystem crossing as well as to vibrational relaxation induced by the helium droplet environment.<sup>7,31</sup> For  $\text{Na}_3$  in the excited  $2^4E'$ -state the spin-flip reaction was observed to occur with a time constant ranging between 1.4 ns for the vibrational ground state and 380 ps for the asymmetric  $\nu_2 = 2$ -vibration. The probability for the spin-flip reaction was found to sensitively depend on the spin-orbit coupling strength. Accordingly, the branching ratio for the occurrence of unreacted

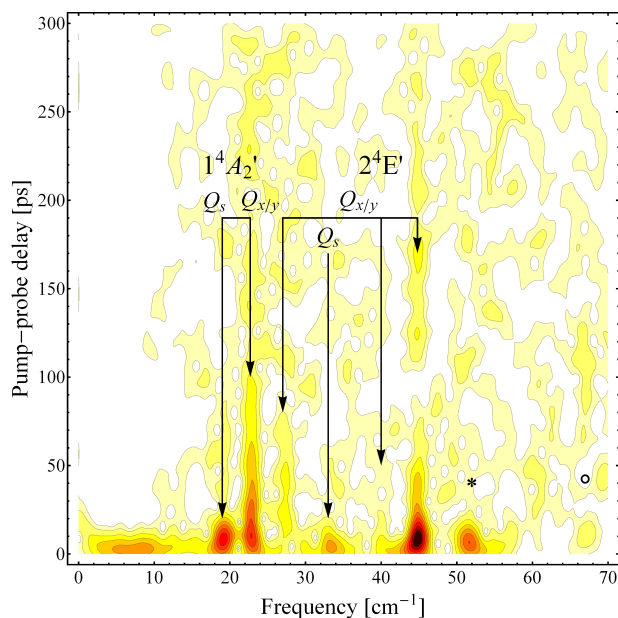


**Fig. 4** Sliding window Fourier analysis of  $\text{Rb}_3$  trimers at 850 nm ( $11765 \text{ cm}^{-1}$ ). The symmetric stretch modes  $Q_s$  are subjected to faster dephasing than the asymmetric modes  $Q_{x/y}$ . Overtone frequencies are marked with a circle, unassigned lines with a star.

trimers and reaction products is significantly shifted toward the spin-flip products in the case of  $\text{K}_3$  as compared to  $\text{Na}_3$ , suggesting significantly shorter spin-flip times. Thus, even faster spin-flip dynamics may be expected for  $\text{Rb}_3$ , which features larger spin-orbit couplings than  $\text{Na}_3$  and  $\text{K}_3$ . Vibrational relaxation of the vibration  $v = 2$  of excited high-spin  $\text{Na}_3$  occurred on a timescale of a few nanoseconds. Possibly, the symmetric ‘breathing’ mode  $Q_s$  considered in our experiments couples more efficiently to the helium environment which would lead to relaxation times in the picosecond range. Note that cw-spectroscopy of larger molecules embedded inside helium nanodroplets indicates that vibronic modes experience variable damping depending on their symmetry.<sup>66</sup> The lack of visible revival structures in Fig. 4 presumably originates from strongly anharmonic potential energy surfaces in combination with limited observation times due to dephasing.

The time-evolution of individual frequency components is extracted from the spectrogram by applying vertical cuts at the line positions and then fitting the temporal data with a single or double exponential decay curve. The corresponding  $1/e$ -lifetimes  $\tau_{1,2}$  are listed in Tables 4 through 7. Due to the limited quality of our data a more sophisticated analysis of the temporal behavior of vibrational modes, which would give insight into the nature of the dephasing process, is not possible.

Additional information for identifying the electronic states involved in the vibrational dynamics is obtained from analyz-

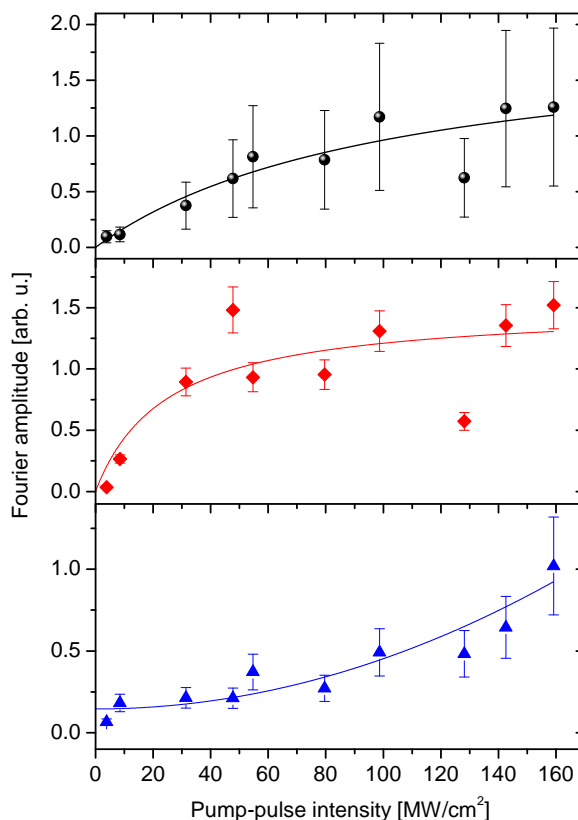


**Fig. 5** Fourier amplitudes for different  $\text{Rb}_3$  frequency components as a function of the pump pulse intensity: upper)  $Q_{x/y}$  mode of the  $1^4A_2'$  lowest quartet state ( $22.7 \text{ cm}^{-1}$ ); middle)  $Q_{x/y}$  mode of the excited  $2^4E'$ -state ( $44.7 \text{ cm}^{-1}$ ); lower) unknown component from higher potential ( $52 \text{ cm}^{-1}$ ).

ing the dependence of the spectral lines on the pump pulse intensity. In the resonant multiphoton excitation and ionization schemes exploited in this study, the amplitudes of spectral components corresponding to vibrations in different electronic states are expected to feature different scaling behavior as a function of excitation laser intensity according to the order of the transition, *i.e.* the number of photons involved. In the experiment, the pump-pulse intensity is varied by placing neutral density filters into the pump beam without changing the position and size of the laser-droplet interaction volume. In order to isolate the pure effect of the pump pulse in the pump-probe scheme, the background count rates, which result from direct 3PI when applying either only the pump or only the probe pulse, are subtracted from the data.

The resulting intensity dependence of the line amplitude at about  $23 \text{ cm}^{-1}$  ( $Q_{x/y}$  modes of  $\text{Rb}_3$  in the  $1^4A_2'$  lowest quar-

tet state), shown in Fig. 5a, is nearly linear, as opposed to clearly non-linear saturation behavior observed for the component at about  $45\text{ cm}^{-1}$  ( $Q_{x/y}$  mode of the excited  $2^4E'$  state), shown in Fig. 5b. This is consistent with the expected lower probability for creating a WP in the quartet ground state  $1^4A_2'$ , which requires a two-photon RISRS-process, as compared to single-photon excitation to the  $2^4E'$ -state. The unassigned broad feature at  $52\text{ cm}^{-1}$ , however, shows an unsaturated non-linearly rising intensity dependence which points at a multiphoton transition to a higher lying state being active. The solid lines represent simple model fit curves to guide the eye.

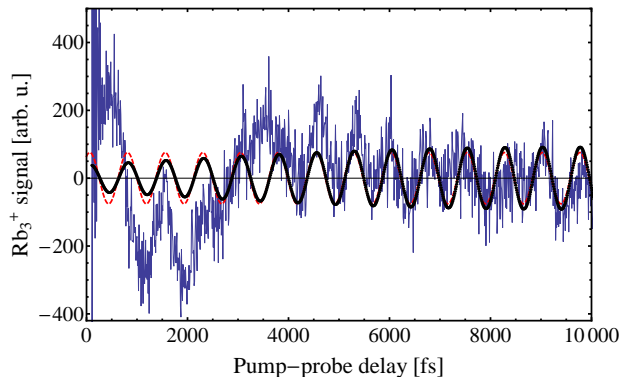


**Fig. 6** Transient signal of  $\text{Rb}_3$  at 850 nm. The black line is obtained by notch filtering the measured total transient at  $44\text{ cm}^{-1}$ . The initial phase is determined from a sinusoidal fit (dashed, red line).

Furthermore, information about the pathway along which the probability density propagates on its way from the initial vibronic ground state up to the final ionic state can be obtained from analyzing the initial phases  $\Phi$  of the individual oscillation components. For the example of a diatomic molecule, when a WP is excited and probed at the same classical turning point of a potential energy curve one expects the phase to be zero, whereas a phase of  $\Phi \approx \pi$  means that the WP is created at one turning point and probed at the other, as observed for the excited state dynamics of  $\text{K}_2$  and  $\text{Rb}_2$  formed on helium nanodroplets.<sup>20,22</sup> The ground state vibrations induced by RISRS in triplet  $\text{Rb}_2$  were found to have initial phases  $\Phi \approx 0.3\ 2\pi$  and  $\Phi \approx 0.7\ 2\pi$  depending on the ionization path which differed from those of the excited state oscillations and thus helped to discern ground and excited state dynamics.<sup>22</sup>

For the determination of initial phases  $\Phi$  in the present measurements, the data are manipulated as follows. A narrow-band notch filter is applied for isolating each frequency component. This is done by multiplying the data in the frequency domain by a narrow gaussian window function ( $1/e^2$ -width of  $0.5\text{ cm}^{-1}$ ) centered around the frequency of interest. The inverse Fourier transform yields the filtered transient data and the initial phase is then obtained from fitting a sinusoidal func-

tion, as illustrated in Fig. 6 for the  $44.7\text{ cm}^{-1}$  component of  $\text{Rb}_3$  excited at 850 nm ( $11765\text{ cm}^{-1}$ ). The resulting initial phases for all prominent lines of all trimer species are shown in Tables 4 through 7 and are discussed in Section 4.

### 3 Theory

For the interpretation of vibrationally resolved spectra a good knowledge of the involved PES is indispensable. In the case of the homonuclear trimers  $\text{K}_3$  and  $\text{Rb}_3$  we fall back to the *ab initio* results of our previous articles on the quartet<sup>34</sup> and doublet<sup>48</sup> states. For our approach to the mixed trimers  $\text{K}_2\text{Rb}$  and  $\text{KRb}_2$  we refer the potential surfaces and the corresponding energy levels of Paper I.<sup>59</sup> Since the alkali metal trimers on the surface of helium droplets are preferably formed in the van der Waals bound high-spin states, we concentrate on the quartet manifold of the electronic states and pick the experimentally relevant states between  $11500$  and  $12100\text{ cm}^{-1}$ . We find that due to the similar electronic state structure of all trimer species the same pair of states, namely  $3^4A_1$  and  $4^4B_2$ , is involved in the electronic excitation. However, for the homonuclear trimers we will use the labels of the  $D_{3h}$  point group because of the increased symmetry at equilateral triangle geometry, where these pairs of states form a doubly degenerate  $2^4E'$  state. The lowest quartet states may be labeled as  $1^4B_2$  in  $C_{2v}$ , corresponding to  $1^4A_2'$  states in  $D_{3h}$ . We will discuss the vibronic spectra predictions for the homo- and heteronuclear trimers in Sections 4.1-4.4.

In the case of the highly symmetric equilateral homonuclear trimers the three normal modes  $Q_s$  (breathing mode),  $Q_x$  (symmetric mode) and  $Q_y$  (asymmetric mode) can be obtained – except for a constant factor – directly from symmetry considerations. They are shown in Figure 7.

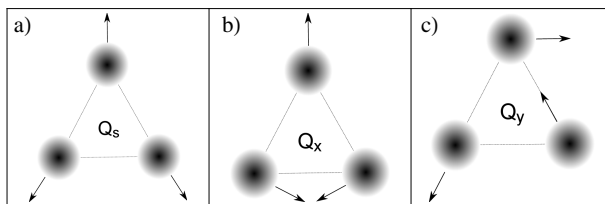


**Fig. 7** Sketched vibrational modes of a homonuclear trimer: (a) symmetric stretch mode, (b) asymmetric bending mode, (c) asymmetric stretch mode.

For the heteronuclear trimers, however, they have to be calculated numerically as described in Paper I.<sup>59</sup> Note that the  $Q_x$  and  $Q_y$  modes are degenerate in the homonuclear trimers, giving rise to a Jahn-Teller distortion in electronically degenerate states. The vibrational degeneracy is lifted by a few wavenumbers in the case of the heteronuclear trimers.



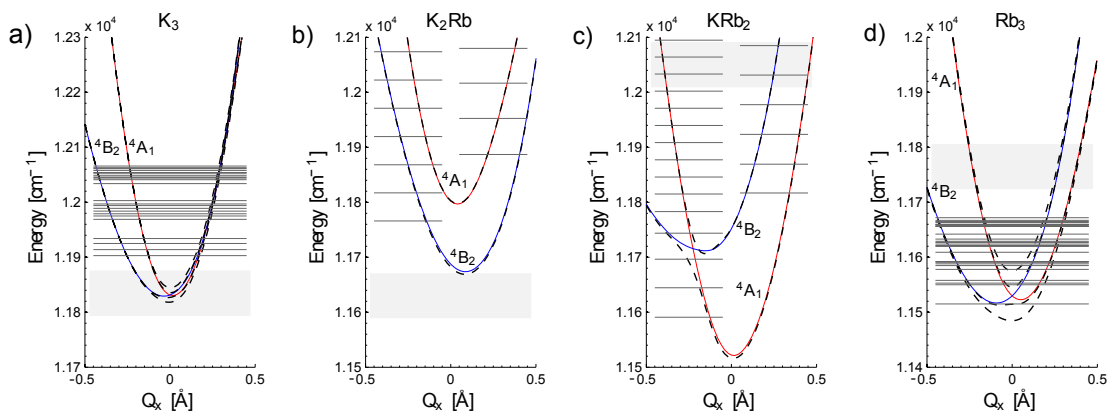


**Fig. 8** Subfigures a)-d) show cuts through the PES of the involved  $3^4A_1$  (red) and  $4^4B_2$  (blue) electronically excited states as a function of  $Q_x$  for all investigated alkali trimers. SO-corrected surfaces are plotted as black-dashed lines. The first few vibronic levels of all SO-PES are indicated by dark grey lines. Experimental laser excitation windows (FWHM of  $80\text{ cm}^{-1}$ ) of prominent power spectra (see Figs. 3, 9, 10 and 11) are plotted as shaded areas. The energy scale is referenced to the vibrational ground state of the  $1^4B_2$  lowest quartet PES.

### 3.1 The $2^4E' \leftarrow 1^4A_2'$ transitions in $K_3$ and $Rb_3$

From previous calculations the electronically excited  $2^4E'$  states of  $K_3$  and  $Rb_3$  with vertical excitation energies of  $11855$  and  $11550\text{ cm}^{-1}$ , respectively, could be identified as the states of major interest for the experimental femtosecond-laser excitation of the homonuclear trimers. In both molecules the  $2^4E'$  state is affected by a combination of Jahn-Teller distortion and spin-orbit coupling. This can be seen in Figures 8a and 8d, where the involved PES for  $K_3$  and  $Rb_3$  are plotted as function of  $Q_x$ . The two branches of the non-relativistic PES can be labeled as  $3^4A_1$  and  $4^4B_2$  in the  $C_{2v}$  point group. Inclusion of SO-coupling leads to a new system of four PES shown as black-dashed lines. In Ref. 34 we provided a detailed analysis of these states in terms of the relativistic Jahn-Teller effect theory and generated spectral simulations for the interpretation of vibrationally resolved experimental data based on a combination of LIF spectroscopy and MCD techniques. For the interpretation of the femtosecond pump-probe data we fall back to the previously calculated vibrational eigenstates in the JT-distorted potential energy surfaces and list them in Tabs. 3 and 9 for  $Rb_3$  and  $K_3$ , respectively. The pump-probe Fourier-spectra are expected to feature difference frequencies between these levels that we will represent as  $(n, m)$  for a beat frequency of levels  $n$  and  $m$ . The most promising candidates in terms of matching frequency differences as well as excitation probabilities are printed in bold. Vibrational excitations of the slightly anharmonic  $Q_s$  mode ( $\nu_{Q_s} \approx 53\text{ cm}^{-1}$  for  $K_3$  and  $33\text{ cm}^{-1}$  for  $Rb_3$ ) are not listed here. The intensities shown in the tables are based on Franck-Condon integrals for transitions from the  $v = 0$  state of the  $1^4A_2'$  lowest quartet state. This information is only weakly related to the much more complex experimental situation of coherent multi-level coupling of dif-

ferent electronically excited states, but may be seen as a zeroth order criteria for the selection of vibronic levels involved. The vibronic levels are also shown in Figure 8 as dark gray lines. Note the high density of levels for the homonuclear trimers caused by SO-splitting.

### 3.2 The $3^4A_1, 4^4B_2 \leftarrow 1^4B_2$ transitions in $K_2Rb$ and $KRb_2$

For the mixed trimers the excited state structure of the quartet manifolds is strongly related to the structure of the homonuclear species in terms of vertical energies and state ordering. This can be seen in Figures 8b and 8c for  $K_2Rb$  and  $KRb_2$ , respectively. The same pairs of states, namely  $3^4A_1$  and  $4^4B_2$ , are involved in the experiment. However, due to the reduction of the molecular symmetry the vibrational degeneracy of  $Q_x$  and  $Q_y$  is lifted and the JT-coupling is suppressed. Nevertheless, the electronic degeneracy remains. In the case of  $KRb_2$  the intersection of the two electronic states lies in the experimentally relevant energy range as can be seen in Figure 8c. The vertical excitation energies are  $11429\text{ cm}^{-1}$  and  $11659\text{ cm}^{-1}$  for the  $3^4A_1$  and the  $4^4B_2$  states of  $KRb_2$ , respectively. In the case of  $K_2Rb$  the same states are found at  $11691\text{ cm}^{-1}$  and  $11577\text{ cm}^{-1}$ , respectively. Following the argumentation given in Paper I<sup>59</sup> the SO coupling can be neglected in the case of the heteronuclear trimers except for the fact that the conical intersection of the two states as a function of  $Q_x$  becomes an avoided crossing. However, this leads, especially for  $KRb_2$ , to a different, strongly anharmonic PES structure with the corresponding vibronic levels listed in Tables 2 and 3 of Paper I.<sup>59</sup>

## 4 Fourier spectra analysis

In this section we compare the measured Fourier spectra with frequencies derived from the *ab initio* calculations. In most cases harmonic approximations to the given potential surfaces are sufficient for a qualitative peak assignment. Therefore, when not specified, given calculated values are the harmonic frequencies to the concerned PES. Exceptions are the Jahn-Teller distorted pairs of excited states in the homonuclear trimers Rb<sub>3</sub> and K<sub>3</sub>, the excited states of KRb<sub>2</sub> due to the avoided crossing in Q<sub>x</sub> and the slightly anharmonic Q<sub>s</sub> modes of all trimers. In the first case we fall back to selected numerical results for the vibronic eigenstates listed in Tables 3 and 9. In the second, we refer to Tables 2 and 3 of Paper I, where a finite-difference approach is applied to solve the nuclear part of the Schrödinger equation explicitly for the given SO-corrected *ab initio* potentials. For the sake of a general overview and a direct comparison the harmonic frequency approximations of all involved states are summarized in Table 2. However, note that the actual structure of vibronic levels (see Tables 3 and 9) in the 2<sup>4</sup>E' states of the homonuclear trimers deviates significantly from the harmonic situation, so the harmonic frequencies in Q<sub>x</sub> and Q<sub>y</sub> are of little value for further interpretations. Instead, particular differences between vibrational levels in the excited states are expected to be present in the Fourier spectra.

**Table 2** Harmonic frequency approximations (in cm<sup>-1</sup>) of all involved quartet states K<sub>2</sub>Rb, KRb<sub>2</sub> (C<sub>2v</sub> point group nomenclature) and Rb<sub>3</sub> and K<sub>3</sub>(D<sub>3h</sub>)

mode	K <sub>3</sub>		K <sub>2</sub> Rb		
	1 <sup>4</sup> A' <sub>2</sub>	2 <sup>4</sup> E'	1 <sup>4</sup> B <sub>2</sub>	3 <sup>4</sup> A <sub>1</sub>	4 <sup>4</sup> B <sub>2</sub>
Q <sub>x</sub>	33	67	34	65	51
Q <sub>y</sub>	33	67	35	57	68
Q <sub>s</sub>	37	52	34	56	49

mode	KRb <sub>2</sub>			Rb <sub>3</sub>	
	1 <sup>4</sup> B <sub>2</sub>	3 <sup>4</sup> A <sub>1</sub>	4 <sup>4</sup> B <sub>2</sub>	1 <sup>4</sup> A' <sub>2</sub>	2 <sup>4</sup> E'
Q <sub>x</sub>	26	54	52	21	42
Q <sub>y</sub>	31	51	62	21	42
Q <sub>s</sub>	28	46	52	19	33

### 4.1 The Rb<sub>3</sub> trimer

The rubidium trimer Rb<sub>3</sub> is the heaviest of the observed species with an average mass of  $m = 255.5$  amu. WP oscillation signals are recorded at different laser wavelengths between about 840 nm (11900 cm<sup>-1</sup>) and 870 nm (11500 cm<sup>-1</sup>) (Fig. 2). The obtained Fourier spectra show multiple vibrational lines with different amplitude and width most of which are visible in a window of about 10 nm around 850 nm (11765 cm<sup>-1</sup>) (Fig. 3). Naively, one would expect a total of 4

lines in the case of the homonuclear trimers: The symmetric Q<sub>s</sub> and the degenerate Q<sub>x/y</sub> modes in the lowest quartet 1<sup>4</sup>A'<sub>2</sub> and in the excited quartet 2<sup>4</sup>E' states.

All relevant spectral information about Rb<sub>3</sub> is compiled in Tab. 4. For the 1<sup>4</sup>A'<sub>2</sub> state the fitted harmonic frequencies of the Q<sub>s</sub> (19 cm<sup>-1</sup>) and the Q<sub>x/y</sub>-modes (21 cm<sup>-1</sup>) are in good agreement with the experimental values, 19.1 cm<sup>-1</sup> and 22.7 cm<sup>-1</sup>. The excited 2<sup>4</sup>E' state shows strong Jahn-Teller and SO couplings which requires a correction of the PES as well as the numerical calculation of vibronic eigenstates for the coupled Q<sub>x/y</sub> modes.<sup>34</sup> As can be seen in Figure 8, at 850 nm (11765 cm<sup>-1</sup>) the laser excitation lies about 200 cm<sup>-1</sup> above the conical intersection, so significant contributions of several excited vibronic levels are expected. Levels of particular interest are those with reasonable FC overlap with the vibrational ground state of the 1<sup>4</sup>A'<sub>2</sub> lowest quartet state.

**Table 3** Positions of vibronic levels (in cm<sup>-1</sup>) in the JT-distorted 2<sup>4</sup>E' electronically excited state of Rb<sub>3</sub>. The harmonic frequency of the degenerate Q<sub>x/y</sub> mode is 42 cm<sup>-1</sup>.

Nr.	abs. position	rel. position <sup>a</sup>	intensity
<b>1</b>	<b>11515</b>	<b>-35</b>	<b>1.42</b>
2	11550	0	0.09
3	11553	3	0.00
<b>4</b>	<b>11558</b>	<b>8</b>	<b>1.14</b>
<b>5</b>	<b>11578</b>	<b>28</b>	<b>0.47</b>
6	11585	35	0.00
7	11588	38	0.16
8	11591	41	0.00
9	11592	42	0.00
0	11609	59	0.00
<b>10</b>	<b>11620</b>	<b>70</b>	<b>0.17</b>
11	11621	71	0.00
12	11624	74	0.02
13	11627	77	0.00
14	11629	79	0.00
<b>15</b>	<b>11633</b>	<b>83</b>	<b>0.70</b>
16	11642	92	0.00
<b>17</b>	<b>11656</b>	<b>106</b>	<b>0.16</b>
18	11657	107	0.00
19	11659	109	0.00
20	11660	110	0.00
21	11663	113	0.00
22	11665	115	0.00
23	11667	117	0.00
<b>24</b>	<b>11672</b>	<b>122</b>	<b>1.36</b>

<sup>a</sup>Energetic difference to the point of the conical intersection, assuming no zero-point energy in Q<sub>s</sub>.

According to the theoretical data listed in Tab. 3 the vibrational frequency beats (1,4) (43 cm<sup>-1</sup>) and (5,10) (42 cm<sup>-1</sup>) are in fair agreement with the experimental peak at 44.7 cm<sup>-1</sup>. Note that – accidentally – this value is also close to the hypo-



thetical value ( $42 \text{ cm}^{-1}$ ) predicted by Jahn-Teller effect theory. However, the full treatment of the problem includes SO-coupling and leads to 4 potential curves with spin projections  $\Sigma = 3/2, 1/2, -1/2, -3/2$ . The states 1 and 4 constituting the (1,4) beat have different spin character. In the case of the  $2^4E'$ -states of  $\text{Rb}_3$  as well as for  $\text{K}_3$  the calculated states in Tables 3 and 9 are just labeled with numbers to refer to their absolute energy and do not represent vibrational quantum numbers. Note that the observed frequency also fits well to a  $\Delta v = 2$  overtone beat of the  $Q_{x/y}$ -mode of the  $1^4A'_2$  PES ( $2 \times 22.7 \text{ cm}^{-1}$ ). This component is observed over a broader band of excitation wavelengths ( $500 \text{ cm}^{-1}$ ) than in the cw excitation spectrum ( $300 \text{ cm}^{-1}$ ) of the same system<sup>12</sup>. This supports the interpretation in terms of a Raman transition to the lowest quartet state  $1^4A'_2$ . However, the combined large laser bandwidth ( $80 \text{ cm}^{-1}$ ) and line broadening due to the high laser intensity can also explain the broadened spectrum with respect to the cw case. Furthermore, it is surprising, that the overtone should be more intensive than the fundamental beat component, which is the case for many of the recorded spectra at other wavelengths not shown in this publication.

The slightly anharmonic symmetric stretch mode  $Q_s$  of the  $2^4E'$ -state is analyzed by integrating the one-dimensional Schrödinger equation. The frequency difference between the lowest vibrational quanta  $v = 0$  and  $v = 1$ , ( $33 \text{ cm}^{-1}$ ) is in very good agreement with the experimental value  $33.4 \text{ cm}^{-1}$ . Generally, the FC factors for the RISRS excitation seem to favor the population of the lowest  $v$ -states. A comparison of the absolute line strengths was not attempted since the higher lying PES involved in the REMPI probing step are yet unknown.

Besides the assigned lines we find a few more peaks in the Fourier spectrum of  $\text{Rb}_3$ . The quite intense line at  $52 \text{ cm}^{-1}$  is attributed to the WP dynamics in a higher lying electronic state that is excited by multiphoton absorption. This interpretation is based on the nonlinear scaling of the line amplitude as a function of pump-laser intensity discussed in Sec. 2.1. Moreover, the initial phase  $\Phi = 0.67(5) 2\pi$  of the WP oscillation at  $52 \text{ cm}^{-1}$  significantly differs from  $\Phi$  of the vibrational transients of the  $1^4A'_2$  and  $2^4E'$ -states. The latter are consistent with  $\Phi = 0$ , indicating coinciding FC-regions for the excitation and the ionization transitions. The weak line at  $66.8 \text{ cm}^{-1}$  may be identified as the first overtone frequency of the  $Q_s$ -mode in the  $2^4E'$ -state ( $33 \text{ cm}^{-1}$ ). Following the suggested approach of picking vibronic levels that have reasonable FC overlap with the lowest vibrational eigenfunction of the  $1^4A'_2$  state one might relate the difference frequencies (15,17) ( $30 \text{ cm}^{-1}$ ) and (15,24) ( $39 \text{ cm}^{-1}$ ) extracted from Table 3 to the weak beats at 27 and  $40 \text{ cm}^{-1}$ , respectively (visible in Fig. 4). Likewise, the weak frequency component at  $60 \text{ cm}^{-1}$  could be related to the calculated frequency (1,5) ( $63 \text{ cm}^{-1}$ ), whereas there is no match for the observed frequency at  $86.6 \text{ cm}^{-1}$ .

The fast decay of the  $Q_s$  modes, visualized in Fig. 4, is consistent with the lifetimes obtained from the line widths of the integral Fourier spectra. As discussed in Sec. 2.1, several ultrafast molecular processes are conceivable, including intramolecular vibrational redistribution (IVR) as observed in the gas-phase,<sup>42,43,45,67</sup> intersystem-crossing or vibrational relaxation induced by the helium droplets, as observed with helium droplet-formed alkali trimers.<sup>7,31</sup> The fact that the  $Q_s$  mode has not been observed in cw spectra of  $\text{Na}_3$  in the gas-phase<sup>38,68</sup> nor with mixed rubidium-potassium trimers formed on helium nanodroplets<sup>12</sup> points at a fast intramolecular process, presumably IVR, to cause the fast decay of the  $Q_s$ -signal.

The  $Q_{x/y}$  mode has a much longer lifetime  $\sim 100 \text{ ps}$ , possibly limited by quartet-doublet intersystem crossing.<sup>7,31</sup> This explains why the cw spectra are entirely dominated by the  $Q_{x/y}$  mode of the excited states. Interestingly, the degenerate mode shows a double exponential decay with two very different time constants. While most of the intensity is lost within a few picoseconds after the excitation, the second decay lasts for hundreds of picoseconds. This leads to a bimodal spectral line structure with a broader base and a nearly Fourier limited central part. This effect could be related to strong initial trimer-droplet interactions followed by the reorganisation of the helium surrounding or desorption of the molecules from the helium droplet surface. Alkali atoms are known to leave the droplets upon electronic excitation and the observed fast decay time is in rough agreement with expected desorption times of about  $10 \text{ ps}$ .<sup>69</sup> The exact value may depend on the dopant species and on the state the dopant is excited to.<sup>27,31,70</sup> Unfortunately, the quality of the recorded data does not allow a more detailed analysis. Future two-color pump-probe experiments will improve the signal quality by choosing appropriate probe frequencies for single-photon PI.

**Table 4** Measured vibrational beat frequencies and calculated frequencies for different vibrational modes in two electronic states of  $\text{Rb}_3$ . The most prominent frequencies are marked in bold.

$\nu_{exp}$ [ $\text{cm}^{-1}$ ]	$\tau_1$ [ps]	$\tau_2$ [ps]	$\Phi$ [ $2\pi$ ]	State (mode)	$\nu_{theo}$ [ $\text{cm}^{-1}$ ]
<b>19.1(2)</b>	16(3)	-	0.08(1)	$1^4A'_2(Q_s)$	19
<b>22.7(3)</b>	33(15)	160(110)	0.15(6)	$1^4A'_2(Q_{x/y})$	21
27	-	-	-	$2^4E'(15, 17)$	30
33.4	-	-	-	$2^4E'(Q_s)$	33
40	-	-	-	$2^4E'(15, 24)$	39
<b>44.7(2)</b>	16(10)	-	0.03(5)	$2^4E'(1, 4)$	42
<b>52(2)</b>	9(1)	-	0.67(5)	-	-
60	-	-	-	$2^4E'(1, 5)$	63
66.8	-	-	-	$2^4E'(Q_s)$	$2 \times 33$
86.6	-	-	-	$2^4E'(1, 4)$	$2 \times 42$

## 4.2 The KRB<sub>2</sub> trimer

Fourier spectra of KRB<sub>2</sub> were recorded in the same way as for Rb<sub>3</sub> but with the quadrupole mass spectrometer set to the mass of KRB<sub>2</sub> (210 amu). Within the tuning range of our Ti:Sapph-laser (730 nm-1050 nm), WP oscillations are visible in the pump-probe transients only between about 820 nm (12200 cm<sup>-1</sup>) and 880 nm (11360 cm<sup>-1</sup>). As seen in the PI-spectrum of Fig. 9, there is an additional feature at 12100 cm<sup>-1</sup> which does not coincide with the first excited quartet states. We assume that this is a REMPI resonance of the pump pulse since we observe the richest WP dynamics in this range. This observation points to the existence of another quartet state in the vicinity of 24200 cm<sup>-1</sup>. We expect one frequency for each of the 3 vibrational modes of the 1<sup>4</sup>B<sub>2</sub> lowest quartet state as well as for the two accessible excited states 3<sup>4</sup>A<sub>1</sub> and 4<sup>4</sup>B<sub>2</sub>. As can be seen in Figure 8c the 3<sup>4</sup>A<sub>1</sub> and 4<sup>4</sup>B<sub>2</sub> excited states of KRB<sub>2</sub> feature a conical intersection in the Q<sub>x</sub> coordinate at -0.2 Å (11600 cm<sup>-1</sup>), which becomes an avoided crossing after inclusion of SO coupling. JT theory does not apply here since electronic degeneracies do not occur at equilateral geometry and the vibrational degeneracy is lifted. Since the experimental excitation at 12050 cm<sup>-1</sup> is well above the crossing point (and 450 cm<sup>-1</sup> above the minimum of the 3<sup>4</sup>A<sub>1</sub> state), the vibrational eigenstates of the SO-corrected adiabatic potential curves used for the interpretation differ significantly from their non-relativistic counterparts. The new states, which can be labeled as E<sub>1/2</sub> states in the C<sub>2v</sub> spin double group, are further referred to as the upper and lower excited quartet PES.

The corresponding power spectrum (Fig. 9) is dominated by two lines at 23 cm<sup>-1</sup> and 31.5 cm<sup>-1</sup>. They are assigned to the Q<sub>x</sub> (26 cm<sup>-1</sup>) and Q<sub>y</sub> (31 cm<sup>-1</sup>) modes of the 1<sup>4</sup>B<sub>2</sub> lowest quartet state and have long lifetimes in the range 150 ps as retrieved from the spectrogram. As in the case of Rb<sub>3</sub> line shapes and spectrograms suggest superimposed fast and slow decays.

The observed vibrational beats at 54.8 cm<sup>-1</sup> and 56.6 cm<sup>-1</sup> roughly coincide with the calculated Q<sub>s</sub> (52 cm<sup>-1</sup>) and Q<sub>x</sub> (52 cm<sup>-1</sup>) modes of the upper quartet PES. The Q<sub>s</sub> modes, however, have low intensities and are shortlived for the examined alkali trimers. Since the upper excited PES is also anharmonic, both observed frequencies could originate from the same Q<sub>x</sub> mode. As can be seen in Figure 8, we should preferentially excite higher *v*-states with non-vanishing FC-factors from the lowest *v*-state in the 1<sup>4</sup>B<sub>2</sub> potential. The calculated beat frequencies are  $\nu_{(1,2)} = 55$  cm<sup>-1</sup>,  $\nu_{(2,3)} = 54$  cm<sup>-1</sup>,  $\nu_{(3,4)} = 53$  cm<sup>-1</sup> and  $\nu_{(4,5)} = 54$  cm<sup>-1</sup>. The beat frequency at 62 cm<sup>-1</sup> fits well to the Q<sub>y</sub> mode (62 cm<sup>-1</sup>) of the upper excited PES. Similar to our approach for Rb<sub>3</sub> we extract the initial phases of the WP oscillations from the pump-probe transients (see Table 5). Within the errors, the states of the 1<sup>4</sup>B<sub>2</sub>

states show phases consistent with zero, whereas beats associated with vibrations on the upper SO-coupled PES show an initial phase of roughly  $\pi$ .

In an alternative approach, we can try to relate many observed frequencies to overtones of the Q<sub>x</sub> and Q<sub>y</sub> modes of the 1<sup>4</sup>B<sub>2</sub> PES, which may be observable because of the high line intensities. We therefore assume the observed beat at 46.1 cm<sup>-1</sup> to be a  $\Delta v = 2$  overtone of the Q<sub>x</sub> mode. The initial phase of this component (0.6(2) 2 $\pi$ ), however, does not match the Q<sub>x</sub> phase (0.05(9) 2 $\pi$ ) and is consistent with the phases of the states on the upper excited PES. Thus, this component may also be associated with Q<sub>s</sub>, Q<sub>x</sub> or Q<sub>y</sub> modes of the upper PES or with vibrations in even higher states. The line at 62 cm<sup>-1</sup> can then alternatively be assigned to a  $\Delta v = 2$  overtone of the 1<sup>4</sup>B<sub>2</sub> Q<sub>y</sub> mode. The remaining line at 93 cm<sup>-1</sup> can be related to a  $\Delta v = 3$  overtone of the same vibrational mode. It is clear from Tabs. 2 and 3 in Paper I that FC-factors are non-zero only for the first few *v*-states in the excited quartet potentials. Since the excitation is hundreds of wavenumbers above the 3<sup>4</sup>A<sub>1</sub> state minimum, we have to excite *v* > 10 in the lower excited PES which is very unlikely. We therefore do not expect to observe any lines originating from the lower PES.

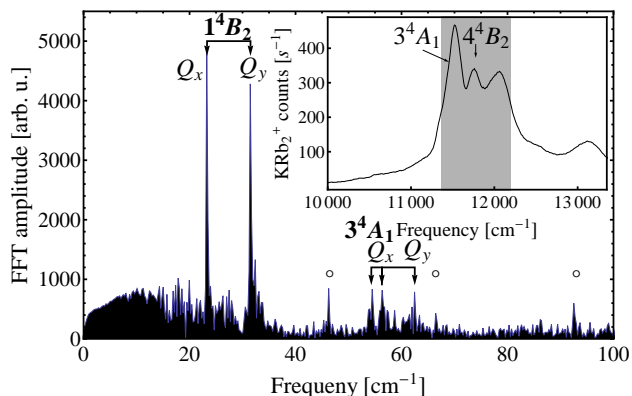


**Fig. 9** Fourier transform of the KRB<sub>2</sub> pump-probe photoionization transient recorded at 830 nm (12048 cm<sup>-1</sup>). The corresponding photoionization spectrum is shown in the inset.

## 4.3 The K<sub>2</sub>Rb trimer

Fourier spectra in the range from 810 nm (12346 cm<sup>-1</sup>) to 870 nm (11494 cm<sup>-1</sup>) were recorded for the lighter mixed trimer K<sub>2</sub>Rb (163.7 amu) which show clearly visible WP dynamics around 860 nm (11630 cm<sup>-1</sup>) as can be seen in Fig. 10. The three lines at lower frequencies are assigned to vibrations in the 1<sup>4</sup>B<sub>2</sub> lowest quartet state where the component at 32.5 cm<sup>-1</sup> agrees reasonably well both with the calculated Q<sub>s</sub> mode (34 cm<sup>-1</sup>) and the Q<sub>x</sub> mode (34 cm<sup>-1</sup>).

**Table 5** Observed vibrational beats of  $\text{KRb}_2$  and calculated values.

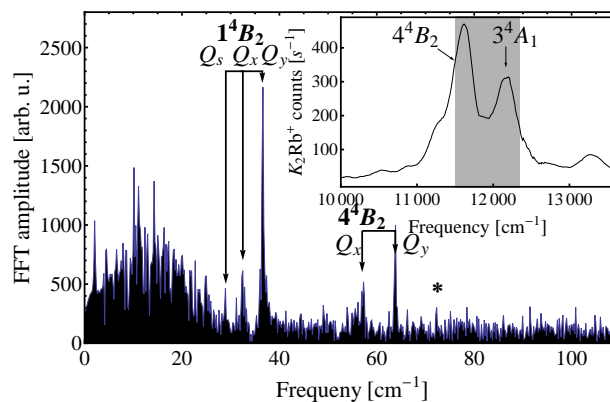
$\nu_{exp}$ [ $\text{cm}^{-1}$ ]	$\tau_1$ [ps]	$\tau_2$ [ps]	$\Phi$ [ $2\pi$ ]	State (mode)	$\nu_{theo}$ [ $\text{cm}^{-1}$ ]
-	-	-	-	$1^4\text{B}_2(\text{Q}_s)$	28
<b>23.1(2)</b>	20(5)	136(44)	0.05(9)	$1^4\text{B}_2(\text{Q}_x)$	26
<b>31.4(2)</b>	19(2)	155(30)	0.2(2)	$1^4\text{B}_2(\text{Q}_y)$	31
46.1(2)	-	470(170)	0.6(3)	$1^4\text{B}_2(\text{Q}_x)$	$2 \times 26$
-	-	-	-	$4^4\text{B}_2(\text{Q}_s)$	52
54.8(5)	-	82(12)	0.6(2)	$4^4\text{B}_2(\text{Q}_x)$ (3, 4)	52
56.6(2)	-	116(15)	0.6(1)	$4^4\text{B}_2(\text{Q}_x)$ (4, 5)	54
62.0(3)	16(1)	240(110)	0.83(17)	$4^4\text{B}_2(\text{Q}_y)$	62
66.5	-	-	-	$1^4\text{B}_2(\text{Q}_x)$	$3 \times 26$
93	-	-	-	$1^4\text{B}_2(\text{Q}_y)$	$3 \times 31$

Since the symmetric stretch modes have been observed to be much weaker than the asymmetric stretch and bending modes for all examined trimers we favor the assignment to the  $\text{Q}_x$  mode. Another weak line is found at  $28.2 \text{ cm}^{-1}$ , but the assignment to the  $\text{Q}_s$  mode is rather speculative. Because of the high intensities of the femtosecond laser in the range of  $1 \text{ GW}/\text{cm}^2$ , one could imagine multiphoton Raman excitation, leading to excitation of higher  $v$ -states in the lowest quartet potential. The latter proves to be quite anharmonic, and an excitation to  $v=4-6$  roughly matches the calculated frequencies ( $\nu_{(4,5)}=30.2 \text{ cm}^{-1}$ ,  $\nu_{(5,6)}=29.5 \text{ cm}^{-1}$  and  $\nu_{(6,7)}=28.8 \text{ cm}^{-1}$ ). The calculations yield a  $\text{Q}_y$  frequency of  $35 \text{ cm}^{-1}$  which is in good agreement with the observed line at  $36.6 \text{ cm}^{-1}$ . The beat note at  $56.3 \text{ cm}^{-1}$  is quite close to the very harmonic  $\text{Q}_x$  ( $51 \text{ cm}^{-1}$ ) mode of the  $4^4\text{B}_2$ -state. Finally, the observed frequency at  $63.8 \text{ cm}^{-1}$  is assigned to vibrations in the  $\text{Q}_y$  mode ( $68 \text{ cm}^{-1}$ ) of the  $4^4\text{B}_2$ -state. In this case, the difference of several wavenumbers between the observed and calculated frequency can be explained by the failure of the harmonic approximation. The finite differences calculation of the first beat frequencies are  $\nu_{(0,1)}=69 \text{ cm}^{-1}$ ,  $\nu_{(1,2)}=67.7 \text{ cm}^{-1}$  and  $\nu_{(2,3)}=66.5 \text{ cm}^{-1}$  and  $\nu_{(3,4)}=61.6 \text{ cm}^{-1}$ . We therefore find a best match for beat frequencies  $\nu_{(2,3)}$  or  $\nu_{(3,4)}$ . The  $\text{Q}_s$  frequency calculation yields a value of  $48 \text{ cm}^{-1}$  and the spectrum suggests that there is a very weak line at this position (see Fig. 10). However, the noise is too large to make a definitive assignment.

As for the case of  $\text{KRb}_2$ , we can try to alternatively relate some of the observed frequencies to  $\Delta v = 2$ -overtones of the modes in the lowest quartet PES  $1^4\text{B}_2$ . Following these lines, the observed frequency difference at  $56.3 \text{ cm}^{-1}$  could be the overtone of the  $\text{Q}_s$  mode ( $28 \text{ cm}^{-1}$ ), and likewise the beat frequency at  $63.8 \text{ cm}^{-1}$  could be the  $\text{Q}_x$  ( $32.5 \text{ cm}^{-1}$ ) overtone. The very weak frequency component at  $72.5 \text{ cm}^{-1}$  might then be the corresponding  $\Delta v = 2$ -beat of the  $\text{Q}_y$  mode ( $36.6 \text{ cm}^{-1}$ ). Unlike for the case of  $\text{KRb}_2$ , though, the inten-

sities of the presumed overtones are mostly higher here than the fundamental frequencies which is not easily understood.

Since the excitation laser frequency of  $11628 \text{ cm}^{-1}$  is tuned to the transition  $4^4\text{B}_2 \leftarrow 1^4\text{B}_2$  we do not expect vibrations of the  $3^4\text{A}_1$ -state which is roughly  $150 \text{ cm}^{-1}$  higher in energy and out of range for the given excitation bandwidth. As for the other species, the WP phases were extracted from the spectrogram data yielding about  $0.3 \cdot 2\pi$  for the  $1^4\text{B}_2$  potential. However, the beat at  $36.0 \text{ cm}^{-1}$ , which is assigned to the  $\text{Q}_y$  mode, is not consistent with this value ( $0.18(2) \cdot 2\pi$ ). The  $4^4\text{B}_2$  excited quartet-state beats are found to have phases of about  $0.6 \cdot 2\pi$ .

**Fig. 10** Fourier transform of the  $\text{K}_2\text{Rb}$  pump-probe photoionization transient at  $860 \text{ nm}$  ( $11630 \text{ cm}^{-1}$ ) with the corresponding photoionization spectrum.**Table 6** Observed vibrational beats of  $\text{K}_2\text{Rb}$  and calculated values.

$\nu_{exp}$ [ $\text{cm}^{-1}$ ]	$\tau_1$ [ps]	$\tau_2$ [ps]	$\Phi$ [ $2\pi$ ]	State (mode)	$\nu_{theo}$ [ $\text{cm}^{-1}$ ]
28.2	-	-	0.30(2)	$1^4\text{B}_2(\text{Q}_s)$	34
32.5(5)	26(29)	-	0.35(2)	$1^4\text{B}_2(\text{Q}_x)$	34
<b>36.6(2)</b>	28(5)	440(200)	0.18(2)	$1^4\text{B}_2(\text{Q}_y)$	35
-	-	-	-	$4^4\text{B}_2(\text{Q}_s)$	49
<b>56.3(4)</b>	-	-	0.7(2)	$4^4\text{B}_2(\text{Q}_x)$	51
<b>63.8(2)</b>	38(2)	-	0.56(16)	$4^4\text{B}_2(\text{Q}_y)$	68

#### 4.4 The $\text{K}_3$ trimer

The Fourier spectrum of the potassium trimer  $\text{K}_3$  ( $117.3 \text{ amu}$ ) at  $840 \text{ nm}$  ( $11835 \text{ cm}^{-1}$ ) depicted in Fig. 11 shows some resemblance to its heavier cousin  $\text{Rb}_3$ . However, peak assignment turns out to be more difficult here. Our suggestions are summarized in Table 7.

Vibrational WP dynamics is observed in a window between  $810 \text{ nm}$  ( $12345 \text{ cm}^{-1}$ ) and  $850 \text{ nm}$  ( $11765 \text{ cm}^{-1}$ ) which cor-

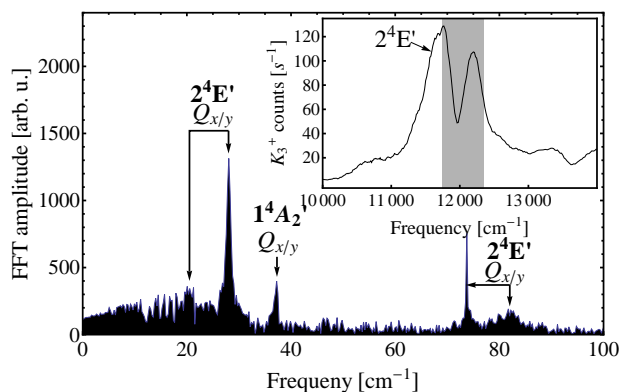


**Fig. 11** Fourier transform of the  $K_3$  pump-probe photoionization transient at 840 nm ( $11835 \text{ cm}^{-1}$ ). The range of the observed WP-dynamics is visualized in gray in the photoionization spectrum (inset)

**Table 7** Observed vibrational beats of  $K_3$  and calculated values.

$\nu_{exp}$ [ $\text{cm}^{-1}$ ]	$\tau_1$ [ps]	$\tau_2$ [ps]	$\Phi$ [ $2\pi$ ]	State (mode)	$\nu_{theo}$ [ $\text{cm}^{-1}$ ]
20	-	-	-	$2^4E'(1,3)$	22
<b>28(2)</b>	18	-	0.14(3)	$2^4E'(1,4)$ or	31
-	-	-	-	$1^4A'_2(Q_s)(3,4)$	33.8
<b>37.1(2)</b>	17(6)	58(25)	0.26(20)	$1^4A'_2(Q_{x/y})(3,4)$	36.1
-	-	-	-	$2^4E'(Q_s)$	53
<b>73.8(2)</b>	21(7)	180(120)	0.14(13)	$2^4E'(1,6)$	72
81.7(2)	7(5)	-	0.48(3)	$2^4E'(1,8)$	81
110.0(5)	9(5)	42	-	-	-

responds to the  $2^4E' \leftarrow 1^4A'_2$  transition,<sup>31,34</sup> but again the richest spectra are obtained within a narrow interval of about 10 nm around 840 nm ( $11905 \text{ cm}^{-1}$ ). When comparing to the  $Rb_3$  spectrum one is led to assign the component at  $28 \text{ cm}^{-1}$  to  $Q_s$  and the beat note at  $37 \text{ cm}^{-1}$  to the  $Q_{x/y}$  mode of the lowest quartet state  $1^4A'_2$ . Beside the qualitative resemblance of the spectra, the wavelength dependence and the lifetime of the observed beats are similar to their counterparts in  $Rb_3$ . The tentatively assigned  $Q_{x/y}$  beat is visible over a wide range of excitation wavelengths ( $400 \text{ cm}^{-1}$ ) whereas the peak at  $28 \text{ cm}^{-1}$  only appears in a window of some  $100 \text{ cm}^{-1}$  around  $11900 \text{ cm}^{-1}$ . The lifetime of the  $Q_s$  beat is 16 ps in the case of  $Rb_3$  and 17 ps for the discussed beat component whereas the  $37 \text{ cm}^{-1}$  beat is observed over longer delay times (58(25) ps).

The calculated harmonic frequencies of the  $Q_{x/y}$  ( $33 \text{ cm}^{-1}$ ) and  $Q_s$  ( $37 \text{ cm}^{-1}$ ), however, do not support this interpretation. A better agreement is achieved when assuming that vibrational states with  $v > 3$  are populated in the anharmonic PES (see Tab. 8) which is imaginable because of the high laser inten-

**Table 8** Calculated beat frequencies (in  $\text{cm}^{-1}$ ) of the  $Q_s$  and  $Q_{x/y}$ -modes in the  $1^4A'_2$  lowest quartet state of  $K_3$ .

Mode	$v = 0, 1$	$v = 1, 2$	$v = 2, 3$	$v = 3, 4$
$Q_s$	37	35.9	34.8	33.8
$Q_{x/y}$	34.1	35.5	35.9	36.1

sities that may drive multiphoton transitions. Alternatively, the beat at  $28 \text{ cm}^{-1}$  can be related to the lowest vibrational levels of the excited  $2^4E'_2$  state (see Figure 8a and Tab. 9). For the first few eigenstates, namely 1, 3, 4, 6 and 8 there is good FC overlap with the lowest vibrational eigenfunction of the  $1^4A'_2$  state and there is a reasonably good match with the calculated component (1,4) ( $31 \text{ cm}^{-1}$ ). Although difficult to detect because of its low frequency there is some experimental evidence for another small peak around  $20 \text{ cm}^{-1}$  which might be related to the beat (1,3) ( $22 \text{ cm}^{-1}$ ). According to Ref. 34 these two smaller beats are caused by coherent excitation of the lowest vibrational states of different spin surfaces, whereas the difference frequencies (1,6) ( $72 \text{ cm}^{-1}$ ) and (1,8) ( $81 \text{ cm}^{-1}$ ) involve fundamental vibrations. The two latter beat components are in good agreement with the experimental peaks at  $73.8 \text{ cm}^{-1}$  and  $81.7 \text{ cm}^{-1}$ . As for the case of  $Rb_3$ , it has to be mentioned that the observed beat at  $73.8 \text{ cm}^{-1}$  can also be related to an overtone of the  $Q_{x/y}$  in the lowest quartet PES  $1^4A'_2$ . The component is observed over a larger wavelength range ( $400 \text{ cm}^{-1}$ ) than the observed width of the cw excitation ( $200 \text{ cm}^{-1}$ ), pointing at a RIRS transition. Just like for  $Rb_3$ , the laser bandwidth and intensity could explain this observation.

As expected, the theoretical value of  $67 \text{ cm}^{-1}$  for the  $Q_{x/y}$ -mode in the JT distorted  $2^4E'$  state does not occur due to SO coupling. The harmonic frequency ( $52 \text{ cm}^{-1}$ ) for  $Q_s$  in the  $2^4E'$  state does not occur either.

## 4.5 Conclusion

In the presented combined experimental and theoretical study we compare measured and *ab initio* calculated vibrational frequencies of quartet states of all triatomic molecules composed of K and Rb atoms. These molecules are formed on the surface of helium nanodroplets and interrogated using femtosecond Fourier spectroscopy. This technique circumvents the considerable spectral perturbations induced by the helium environment that limit the resolution of linear spectroscopy by probing vibrational coherences in the time-domain. Thus, vibrational beat frequencies can be determined with high precision of the order  $0.2 \text{ cm}^{-1}$ .

In contrast to the straight forward assignment of pump-probe power spectra recorded for diatomic alkali molecules<sup>20,22</sup>, the interpretation of vibrational spectra of alkali trimers turns out

**Table 9** Positions of vibronic levels (in  $\text{cm}^{-1}$ ) in the JT-distorted  $2^4E'$  electronically excited state of  $\text{K}_3$ . The harmonic frequency of the degenerate  $Q_{x/y}$  mode is  $67 \text{ cm}^{-1}$ .

Nr.	abs. position	rel. position <sup>a</sup>	intensity
<b>1</b>	<b>11903</b>	<b>48</b>	<b>3.97</b>
2	11914	59	3.59
<b>3</b>	<b>11925</b>	<b>70</b>	<b>3.50</b>
<b>4</b>	<b>11934</b>	<b>79</b>	<b>3.55</b>
5	11969	114	0.00
<b>6</b>	<b>11975</b>	<b>120</b>	<b>0.50</b>
7	11979	124	0.00
<b>8</b>	<b>11984</b>	<b>129</b>	<b>0.21</b>
9	11989	134	0.00
1	11994	139	0.13
11	11997	142	0.00
12	12003	148	0.13
13	12034	179	0.00
14	12041	186	0.39
15	12044	189	0.00
16	12046	191	0.00
17	12049	194	0.38
18	12053	198	0.00
19	12054	199	0.00
20	12058	203	0.37
21	12061	206	0.00
22	12063	208	0.00
23	12066	211	0.37

<sup>a</sup>Energetic difference to the point of the conical intersection, assuming no zero-point energy in  $Q_s$ .

to be much more involved due to a complex interplay of JT and SO-couplings. Moreover, the amplitudes of the observed beat components cannot be analyzed easily because of the Raman-type multiphoton excitations and ionizations via unknown higher electronic states. Therefore, in many cases the assignment of experimental frequencies to calculated values has to be considered as tentative.

Nevertheless, we suggest assignments of the measured beat frequencies to vibrational modes of the lowest and excited quartet states by taking several experimental observables into consideration, including line positions and widths, laser intensity-dependences and mode-specific ultrafast dynamics. The agreement with vibrational frequencies obtained from high-level *ab initio* calculations that include Jahn-Teller and spin-orbit perturbations is satisfactory in the cases of  $\text{Rb}_3$ ,  $\text{KRb}_2$ , and  $\text{K}_2\text{Rb}$ . Most prominent lines in the Fourier spectra of these molecules are the asymmetric stretch and bending modes  $Q_{x/y}$  of the lowest quartet state excited by impulsive Raman scattering, followed by the  $Q_{x/y}$ -modes of the accessible excited electronic states. The breathing mode  $Q_s$  is only visible in the spectrum of  $\text{Rb}_3$ , where it is significantly broadened due to fast dephasing within a few ps. Intramolecular vibrational

relaxation, intersystem-crossing or vibrational relaxation by coupling to the helium environment may be at the origin of this fast dynamics. In contrast, the  $Q_{x/y}$ -modes feature long coherence times of the order of 100 ps. In the case of  $\text{K}_3$  several frequencies can not be assigned unambiguously. The presented spectroscopic data are expected to serve as valuable input information for upcoming experiments aiming at forming ultracold triatomic molecules in optical traps and lattices.

## Acknowledgments

We thank C. Callegari for valuable discussion and DFG for financial support. AWH gratefully acknowledges support from the Graz Advanced School of Science, a cooperation project between TU Graz and the University of Graz, and the Austrian Science Fund (FWF, Grant No. P19759-N20).

## References

- 1 J. P. Toennies and A. F. Vilesov, *Angewandte Chemie*, 2004, **43**, 2622–2648.
- 2 F. Stienkemeier and K. Lehmann, *J. Phys. B*, 2006, **39**, R127.
- 3 J. Tiggesbäumker and F. Stienkemeier, *Phys. Chem. Chem. Phys.*, 2007, **9**, 4748.
- 4 C. Callegari and W. E. Ernst, in *Handbook of High-Resolution Spectroscopy*, ed. M. Quack and F. Merkt, Wiley-VCH, 2011.
- 5 M. Hartmann, R. E. Miller, J. P. Toennies and A. Vilesov, *Phys. Rev. Lett.*, 1995, **75**, 1566–1569.
- 6 J. Higgins, C. Callegari, J. Reho, F. Stienkemeier, W. E. Ernst, M. Gutowski and G. Scoles, *J. Phys. Chem.*, 1998, **102**, 4952–4965.
- 7 J. Higgins, C. Callegari, J. Reho, F. Stienkemeier, W. E. Ernst, K. K. Lehmann, M. Gutowski and G. Scoles, *Science*, 1996, **273**, 629–631.
- 8 J. Higgins, W. E. Ernst, C. Callegari, J. Reho, K. K. Lehmann and G. Scoles, *Phys. Rev. Lett.*, 1996, **77**, 4532–4534.
- 9 M. Mudrich, O. Bünermann, F. Stienkemeier, O. Dulieu and M. Weidemüller, *Eur. Phys. J. D*, 2004, **31**, 291–299.
- 10 O. Bünermann, M. Mudrich, M. Weidemüller and F. Stienkemeier, *J. Chem. Phys.*, 2004, **121**, 8880–8886.
- 11 O. Bünermann, G. Droppelmann, A. Hernando, R. Mayol and F. Stienkemeier, *jpca*, 2007, **111**, 12684.
- 12 J. Nagl, G. Auböck, A. W. Hauser, O. Allard, C. Callegari and W. E. Ernst, *Phys. Rev. Lett.*, 2008, **100**, 063001.
- 13 F. R. Brühl, R. A. Miron and W. E. Ernst, *J. Chem. Phys.*, 2001, **115**, 10275–10281.

- 14 W. E. Ernst, R. Huber, S. Jiang, R. Beuc, M. Movre and G. Pichler, *J. Chem. Phys.*, 2006, **124**, 024313.
- 15 C. P. Schulz, P. Claas and F. Stienkemeier, *Phys. Rev. Lett.*, 2001, **87**, 153401.
- 16 G. Droppelmann, M. Mudrich, C. P. Schulz and F. Stienkemeier, *Eur. Phys. J. D*, 2009, **52**, 67–70.
- 17 C. P. Schulz, P. Claas, D. Schumacher and F. Stienkemeier, *Phys. Rev. Lett.*, 2004, **92**, 013401.
- 18 G. Droppelmann, O. Bünermann, C. P. Schulz and F. Stienkemeier, *Phys. Rev. Lett.*, 2004, **93**, 0233402.
- 19 M. Mudrich, G. Droppelmann, P. Claas, C. Schulz and F. Stienkemeier, *Phys. Rev. Lett.*, 2008, **100**, 023401.
- 20 P. Claas, G. Droppelmann, C. P. Schulz, M. Mudrich and F. Stienkemeier, *J. Phys. B: At. Mol. Opt. Phys.*, 2006, **39**, S1151.
- 21 P. Claas, G. Droppelmann, C. P. Schulz, M. Mudrich and F. Stienkemeier, *J. Phys. Chem. A*, 2007, **111**, 7537.
- 22 M. Mudrich, P. Heister, T. Hippler, C. Giese, O. Dulieu and F. Stienkemeier, *Phys. Rev. A*, 2009, **80**, 042512.
- 23 S. Grebenev, J. P. Toennies and A. F. Vilesov, *Science*, 1998, **279**, 2083–2085.
- 24 B. Dick and A. Slenczka, *J. Chem. Phys.*, 2001, **115**, 10206–10213.
- 25 G. Auböck, M. Aymar, O. Dulieu and W. E. Ernst, *J. Chem. Phys.*, 2010, **132**, 054304.
- 26 G. Auböck, J. Nagl, C. Callegari and W. E. Ernst, *J. Phys. Chem. A*, 2007, **111**, 7404–7410.
- 27 B. Grüner, M. Schlesinger, P. Heister, W. T. Strunz, F. Stienkemeier and M. Mudrich, *Phys. Chem. Chem. Phys.*, 2011, **13**, 6816–6826.
- 28 M. Schlesinger, M. Mudrich, F. Stienkemeier and W. T. Strunz, *Chem. Phys. Lett.*, 2010, **490**, 245.
- 29 M. Koch, G. Auböck, C. Callegari and W. E. Ernst, *Phys. Rev. Lett.*, 2009, **103**, 035302.
- 30 J. Higgins, T. Hollebeek, J. Reho, T.-S. Ho, K. K. Lehmann, H. Rabitz and G. Scoles, *J. Chem. Phys.*, 2000, **112**, 5751–5761.
- 31 J. Reho, J. Higgins, M. Nooijen, K. K. Lehmann, G. Scoles and M. Gutowski, *J. Chem. Phys.*, 2001, **115**, 10265–10274.
- 32 G. Auböck, J. Nagl, C. Callegari and W. E. Ernst, *J. Chem. Phys.*, 2008, **129**, 114501.
- 33 J. Nagl, G. Auböck, A. Hauser, O. Allard, C. Callegari and W. Ernst, *J. Chem. Phys.*, 2008, **128**, 154320.
- 34 A. W. Hauser, G. Auböck, C. Callegari and W. E. Ernst, *J. Chem. Phys.*, 2010, **132**, 164310.
- 35 A. W. Hauser, C. Callegari and W. E. Ernst, in *Advances in the Theory of Atomic and Molecular Systems*, ed. W. N. Lipscomb, I. Prigogine, P. Piccuch, J. Maruani, G. Delgado-Barrio and S. Wilson, Springer Netherlands, 2009, vol. 20, pp. 201–215.
- 36 A. W. Hauser, G. Auböck and W. E. Ernst, in *Vibronic Interactions and the Jahn-Teller Effect II: Applications*, ed. C. Daul, Springer, 2011, in press.
- 37 M. Theisen, F. Lackner and W. E. Ernst, *J. Phys. Chem. A*, 2011, in press.
- 38 W. E. Ernst and S. Rakowsky, *Phys. Rev. Lett.*, 1995, **74**, 58–61.
- 39 W. E. Ernst and O. Golonzka, *Physica Scripta*, 2004, **T112**, 27–32.
- 40 T. Baumert, R. Thalweiser and G. Gerber, *Chem. Phys. Lett.*, 1993, **209**, 29.
- 41 H. Ruppe, S. Rutz, E. Schreiber and L. Wöste, *Chem. Phys. Lett.*, 1996, **257**, 356.
- 42 B. Reischl, *Chem. Phys. Lett.*, 1995, **239**, 173.
- 43 B. Reischl, R. de Vivie-Riedle, S. Rutz and E. Schreiber, *J. Chem. Phys.*, 1996, **104**, 8857–8864.
- 44 S. Rutz and E. Schreiber, *Chem. Phys. Lett.*, 1997, **269**, 9.
- 45 E. Schreiber, *Femtosecond Real-Time Spectroscopy of Small Molecules and Clusters*, Springer, Heidelberg, 1998.
- 46 A. W. Hauser, C. Callegari, P. Soldán and W. E. Ernst, *J. Chem. Phys.*, 2008, **129**, 44307.
- 47 M. Gruebele and A. H. Zewail, *J. Phys. Chem.*, 1992, **98**, 883.
- 48 A. W. Hauser, C. Callegari, P. Soldán and W. E. Ernst, *J. Chem. Phys.*, 2010, **375**, 73–84.
- 49 G. Quémener, P. Honvault, J.-M. Launay, P. Soldan, D. E. Potter and J. M. Hutson, *Phys. Rev. A*, 2005, **71**, 032722.
- 50 P. Soldán, M. T. Cvitaš and J. M. Hutson, *Phys. Rev. A*, 2003, **67**, 054702.
- 51 F. Lang, K. Winkler, C. Strauss, R. Grimm and J. H. Denschlag, *Phys. Rev. Lett.*, 2008, **101**, 133005.
- 52 K.-K. Ni, S. Ospelkaus, M. H. G. de Miranda, A. Pe’er, B. Neyenhuis, J. J. Zirbel, S. Kotochigova, P. S. Julienne, D. S. Jin and J. Ye, *Science*, 2008, **322**, 231.
- 53 J. G. Danzl, M. J. Mark, E. Haller, M. Gustavsson, R. Hart, J. Aldegunde, J. M. Hutson and H.-C. Nägerl, *Nat. Phys.*, 2010, **6**, 265.
- 54 R. V. Krems, *Phys. Chem. Chem. Phys.*, 2008, **10**, 4079.
- 55 M. T. Bell and T. P. Softley, *Mol. Phys.*, 2009, **107**, 99.
- 56 J. Hutson, *Science*, 2010, **327**, 788.
- 57 S. Knoop, F. Ferlaino, M. Berninger, M. Mark, H.-C. Nägerl, R. Grimm, J. P. D’Incao and B. D. Esry, *Phys. Rev. Lett.*, 2010, **104**, 053201.
- 58 S. Ospelkaus, K.-K. Ni, D. Wang, M. H. G. de Miranda, B. Neyenhuis, G. Quémener, P. S. Julienne, J. L. Bohn, D. S. Jin and J. Ye, *Science*, 2010, **327**, 853.
- 59 A. W. Hauser and W. E. Ernst, *Phys. Chem. Chem. Phys.*, 2011, submitted.

- 
- 60 O. Bünermann and F. Stienkemeier, *The European Physical Journal D - Atomic, Molecular, Optical and Plasma Physics*, 2011, **61**, 645–655.
- 61 F. Dalfovo, *Z. Phys. D*, 1994, **29**, 61–66.
- 62 F. Ancilotto, G. DeToffol and F. Toigo, *Phys. Rev. B*, 1995, **52**, 16125–16129.
- 63 F. Stienkemeier, J. Higgins, C. Callegari, S. I. Kanorsky, W. E. Ernst and G. Scoles, *Z. Phys. D*, 1996, **38**, 253–263.
- 64 T. Baumert, R. Thalweiser, V. Weiss and G. Gerber, *Z. Phys. D*, 1993, **26**, 131.
- 65 A. Ruff, S. Rutz, E. Schreiber and L. Wöste, *Zeitschrift für Physik D Atoms, Molecules and Clusters*, 1996, **37**, 175–180.
- 66 R. Lehnig and A. Slenczka, *The Journal of Chemical Physics*, 2003, **118**, 8256–8260.
- 67 S. Rutz, H. Ruppe and E. Schreiber, *Z. Phys. D*, 1997, **40**, 25–29.
- 68 A. Herrmann, M. Hofmann, S. Leutwyler, E. Schumacher and L. Wöste, *Chem. Phys. Lett.*, 1979, **62**, 216.
- 69 T. Takayanagi and M. Shiga, *Chem. Phys. Lett.*, 2003, **372**, 90.
- 70 G. Auböck, J. Nagl, C. Callegari and W. E. Ernst, *Phys. Rev. Lett.*, 2008, **101**, 035301.